Hierarchical salt-ceramic composites for efficient thermochemical energy storage

Lucie Tabard, Elodie Prud'Homme, Vincent Garnier, Laurent Gremillard

Hierarchical Salt-Ceramic Composites for Efficient Thermochemical Energy Storage.

Published in Applied Materials Today 20 (2020), article number 100658
https://doi.org/10.1016/j.apmt.2020.100658

Lucie TABARD[a], Elodie PRUD'HOMME[a], Vincent GARNIER[a], Laurent GREMILLARD[a,*]
[a] Univ Lyon, INSA-Lyon, CNRS, MATEIS UMR5510, 7 Av. Jean Capelle, F-69621 Villeurbanne, France;

Lucie Tabard : Lucie.tabard@insa-lyon.fr
Elodie Prud'Homme : Elodie.prudhomme@insa-lyon.fr
Vincent Garnier : Vincent.garnier@insa-lyon.fr
* Correspondig author; E-mail: laurent.gremillard@insa-lyon.fr

Abstract

The performance of a hygroscopic salt (MgSO4, xH2O) used for thermochemical energy storage can be vastly enhanced when it is distributed in a host zirconia ceramic matrix presenting adequate, hierarchized porosity. The host materials were fabricated by a combination of additive manufacturing technique (robocasting) with pore-former additions and partial sintering, to obtain a 3-scale porosity (with pore diameters spread over 3 decades from 200 nm to 200 µm). The composites were then obtained by simple infiltration of the host material by aqueous salt solutions. The porosity enabled to maximize the amount of salt stored in the host material and its accessibility to water vapor, resulting in potentially high energy density (up to 420 $kWh \cdot m^{-3}$), without efficiency loss upon hydration/dehydration cycles.

Keywords

Robocasting; Hierarchized porosity; Zirconia; thermochemical heat storage; magnesium sulfate

1. Introduction

In 2017 renewable energy represented 17.5 % of the energy consumed in the EU, on a path to the 2020 target of 20 % and to the new binding renewable energy target for the EU for 2030 of at least 32% [1,2]. Solar energy, if efficiently harvested, could cover entirely Europe's energy needs [3], thus is to become a very important energy source over the next years. However the time shift between production (summer, daylight) and usage (winter, night) makes it necessary to devise efficient energy storage devices. Thermochemical energy storage could be one of the most efficient ways to store solar heat [4]. It is most often based on the reversible hydration and dehydration of a salt by water vapor. During the charging phase, the solar heat is used to dehydrate the salt. Conversely, the highly exothermic hydration of the salt can produce a large amount of heat [5]. Devices based on this principle (containing hygroscopic salts as active materials, enclosed in a reactor providing both control of the hydration / dehydration conditions and heat extraction and transport) can be used for heating buildings, one of the applications identified by EU who fixed for such devices a 300 $kWh \cdot m^{-3}$ energy density target for 2020 [6].

Strong requirements on price, availability, safety and efficiency limit the choice of salts to only a few (mainly $SrBr_2$, $LaCl_2$, $MgSO_4$) [7]. In particular $MgSO_4$ presents the advantages of being very cheap, much safer than all other salts while offering one of the highest potential energy density [7].

Early prototypes of these reactors consist of stacks of salt beds as reactive solid separated by structures providing both mechanical support and a path for water vapor circulation [8,9]. These systems maximize the amount of salt, thus potentially the energy density. However, their energy efficiency rapidly decreases (from approximately 320 $kWh \cdot m^{-3}$ (72% of the theoretical energy density) during the first hydration / dehydration cycle to ~180 $kWh \cdot m^{-3}$ (41%) during the 7^{th} cycle) [10]. The very limited stability during hydration / dehydration cycles on large-scale reactors, resulting in a drop in energy efficiency, is due to difficulties to maintain the salt in place and to its powdering and agglomeration that result in a global decrease of their porosity and permeability. To overcome these issues, one promising idea is to anchor and distribute the salt in a strong, inert, porous host material, enabling both to maintain a porous path through the whole salt over time and to avoid matrix crumbling and salt agglomeration. Composites made of zeolite and salt are one of the very few examples of such approaches. However, the very small pore size (~1 nm) of the zeolite limits the access of water vapor to the impregnated salt, thus the kinetic and efficiency of the hydration reaction [11,12]. This results in moderate energy density: for example zeolite and 15 wt.%$MgSO_4$ provided 166 $kWh \cdot m^{-3}$, still higher than the energy density stored by water adsorption on zeolite alone (~131 $kWh \cdot m^{-3}$) but far from the complete potential of the composite (~45% efficiency). Therefore, reaching the targeted high energy density of 300 kWh m^{-3} is difficult because it requires a high volume fraction of salt easily accessible to water vapor over time, which thus requires a delicate balance between pore size, porosity and mechanical properties of the host material.

In the present article, a new porous ceramic host material is proposed, taking advantage of the unique possibilities offered by a combination of additive fabrication process (robocasting) with a traditional pore-former method and partial sintering schedules. The three scales of porosity it offers provide sufficient mechanical properties, adequate space to store the salt and enough residual porosity to enable the flow of the reactive gas through the material. A demonstrator is presented here, using ceria-stabilized zirconia as the host ceramic and magnesium sulfate as the active salt. As a results, energy densities as high as 420 $kWh \cdot m^{-3}$, stable over time were obtained.

2. Materials and Methods

2.1. Processing:

Printing pastes were made of 12 vol.% zirconia powder (Daiichi Ce-Z12, 0.5 µm particle size) and 24 vol% wheat starch (Fisher Chemical, extra pure, only for material ZW) dispersed in a Pluronic® F-127 (Sigma-Aldrich) 25 wt.% solution in DI water and Darvan 821A (R.T. Vanderbilt, Norwalk, CT, 0.5 wt/wt % *vs* zirconia), mixed together in a fast planetary mixer (SpeedMixer, Synergy devices limited). In this composition, Darvan 821A was a dispersant of the ceramic powder, and Pluronic® F-127 induced a shear thinning behavior necessary for printing. The pastes were then introduced in 5 mL syringes and de-aired by centrifugation. The robocasting process was conducted using a Robocasting machine (3D-Inks LLC, Tulsa, OK, USA). Briefly, the printing paste contained in the syringe was extruded through a 410 µm needle, the position of which was controlled in 3D over time to reproduce a predefined (CAD) design (here a structure made by piling up layers made of parallel, separate filaments, with a 90° disorientation between two successive layers). Following printing, the support materials where dried in a humidity-controlled chamber (WKL 150, Weiss Technik, France), in order to remove progressively water without cracking the components. A debinding step followed in order to remove all organic components (Pluronic® F-127 and Darvan 821A) (0.5 °C·min^{-1} up to 350 °C, 2 °C·min^{-1} up to 600 °C and a dwell of 2 hours at 600 °C). Finally the samples were sintered in air (5·°C min^{-1} up to 800 °C; 3 °C·min^{-1} up to 1000 °C; 1 °C·min^{-1} up to 1250 °C and a dwell of two hours at 1250 °C). This sintering schedule (low temperature and slow heating ramps) was chosen to favor the growth of necks between the ceramic particles without densifying too much, thus maintaining a large porosity with still reasonable mechanical properties. The host materials were then infiltrated by $MgSO_4$,$7H_2O$ aqueous solutions (710 g·L^{-1}), either at atmospheric pressure (Zi) or under vacuum (ZWv), followed by drying at 150°C for 8 hours. Vacuum infiltration enabled to load larger amount of salts into the host materials; however it was only used to infiltrate ZW material because it resulted in the fracture of Z material.

2.2. Characterization:

Microstructural observations were conducted with a Supra 55 VP scanning electron microscope (SEM, Zeiss, Germany) at 2 kV and a working distance of 2 mm. The overall porosity was determined by measuring the weight and outer volume of the samples. The shape and total volume of the large pores were determined from X-ray microtomography (GE V|Tome X). The small and intermediate pores were assessed by Mercury Intrusion Porosimetry (MIP, Autopore V, Micromeritics, GA, USA) after fitting each pore family with a log-normal distribution. The different phases of $MgSO_4$ where identified by X-Ray Diffraction (Bruker D8 Advance, Cu Kα radiation, LynxEye 1D detector). During hydration and de-hydration cycles of the salt-support material composites, the transitions between phases were monitored by weight measurements (0.1 mg weighting scale), always by comparison with a control support material sample of same structure to take into account possible water adsorption on the support material.

Compressive strength of the host materials was measured with an Instron electro-mechanic universal testing machine (Instron 8500+, Elancourt, France) with a 5 kN load cell, at 0.033 mm·s^{-1} crosshead speed.

3. Results

For this proof-of-concept article, zirconia ceramic was chosen for the fabrication of the porous support materials. Indeed zirconia offers the highest mechanical properties among

monolithic oxide materials. Stabilization with Ceria also results in a larger resistance to humidity than the more known yttria-stabilized zirconia. Robocasting combined to the use of wheat starch as pore-former and a low sintering temperature enabled obtaining Ceria-stabilized zirconia support materials with three levels of porosity. The large pores (ca. 200 µm) are determined by the CAD (Computer-Aided Design) file used for robocasting (thus can be tailored to the user's need). The intermediate porosity (pore size 13 µm, access diameter 2 µm) is determined by the size of the starches particles thus can be varied by changing the type and amount of starch (although only the results for wheat starch are shown here, materials were also successfully processed using potato and rice starch). The small porosity (diameter 0.2 µm) is left by incomplete densification, thus controlled by the sintering thermal cycle. Figure 1 shows a host ceramic (labeled ZW) with 82% porosity (18% for large pores, 51% for intermediate pores, 13% for small pores). For comparison sake, another material (labeled Z) with the same design and thermal treatment but without starch was fabricated (with 66% porosity: 33% for large pores, 33% for small pores).

Compressive strength of 10 MPa and 0.4 MPa were measured for Z and ZW materials respectively.

This combination of processes thus offers a highly tunable platform allowing the fabrication of host ceramic with three scales of porosity variable in range and quantity.

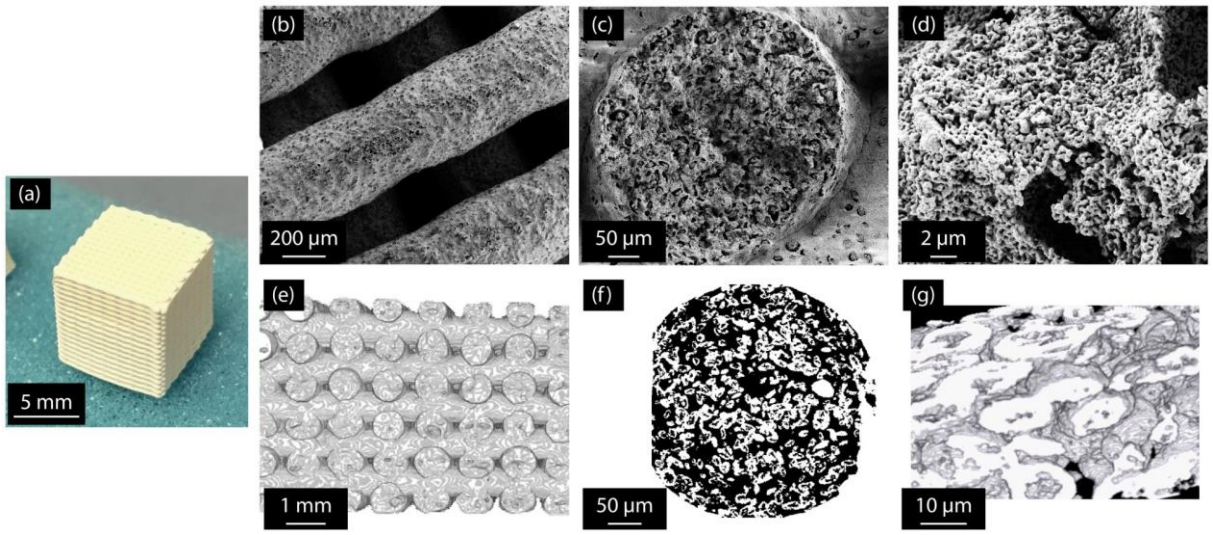

Figure 1: a. ZW after sintering; b.c.d SEM micrographs of ZW microstructure; e. 3D reconstruction of X-ray tomogram (voxel size: 7 µm); f. Thresholded X-ray tomogram slice of the cross section of a filament (ZW); g. 3D reconstruction of the intermediate porosity of ZW from X-ray tomogram (voxel size: 0.3 µm); in f. and g. pores are shown in white.

Supersaturated $MgSO_4$ salt solution was infiltrated in the porous host ceramic. Figure 2 shows that the supersaturated solution can access the whole material, the salt (grey) being found in the core of the filaments of the host materials. As a result after drying the supersaturated solution (*i.e.* eliminating the free water), in the ZW material (labeled ZWv after vacuum infiltration) ~75% of the porosity is occupied by hydrated salt ($MgSO_4$, $7H_2O$). In contrast in the Z material (labeled Zi after atmospheric pressure infiltration), less than 40% of the porosity is occupied by salt. In both cases, open porosity remains.

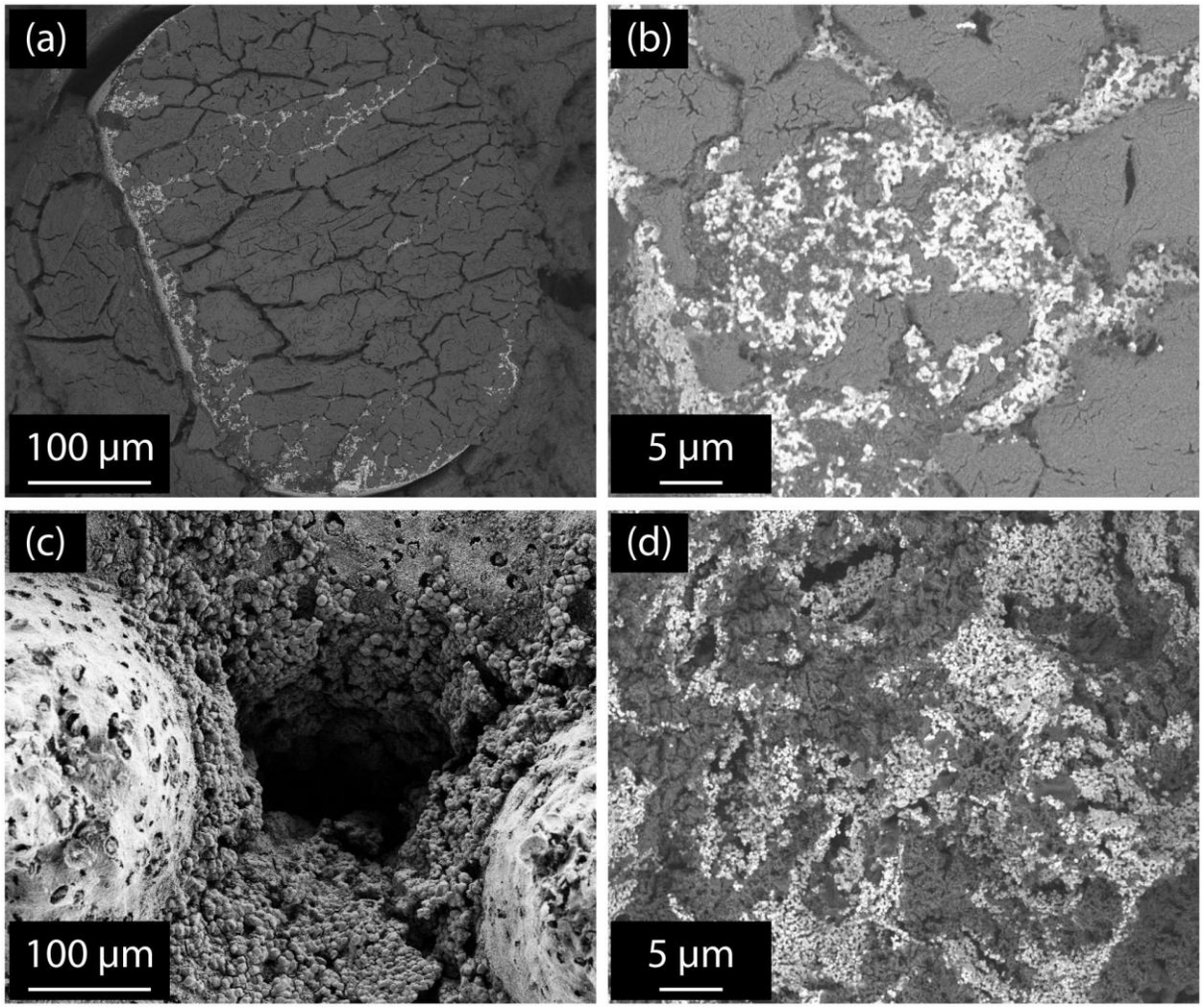

Figure 2: a. Surface of filament Zi, showing a homogeneous but cracked layer of salt on the surface of the filament; b. Fracture surface of filament Zi, showing homogenous infiltration of salt (dark grey) inside small porosity of the zirconia structure (light grey) (large salt areas are due to salt protruding from the material because of natural hydration during storage after fracture). c. Surface of filament ZWv, showing salt heterogeneously spread in the large porosity, and access pores to the intermediate porosity network on the surface of a filament; d. Fracture surface of filament ZWv, showing the salt occupying part of intermediate and small pores.

To assess their resistance to the hydration/dehydration cycles encountered during operation, these salt-host ceramic composites were subjected to 10 cycles of dehydration (150°C, 30% relative humidity) and hydration (room temperature, 98% relative humidity). 10 cycles are believed to be sufficient to notice if any evolution of the composite occurs over time in order to validate the demonstrator efficiency. X-ray diffraction analyses and weight measurements showed that after the dehydrations step, the salt was systematically in its monohydrate state ($MgSO_4,H_2O$). After the hydration steps, the salt systematically reached its hepta-hydrated state. With a 7-1 hydration heat of 667 $kWh \cdot m^{-3}$, and considering the amount of salt in the composite described above, this corresponds to 177 and 417 $kWh \cdot m^{-3}$ respectively for Zi and ZWv materials (Figure 3). Note that the ZW material without salt (also shown in Figure 3) does not gain or lose mass with hydration / dehydration steps, showing that adsorption of water molecules onto the host material, if any, is not significant.

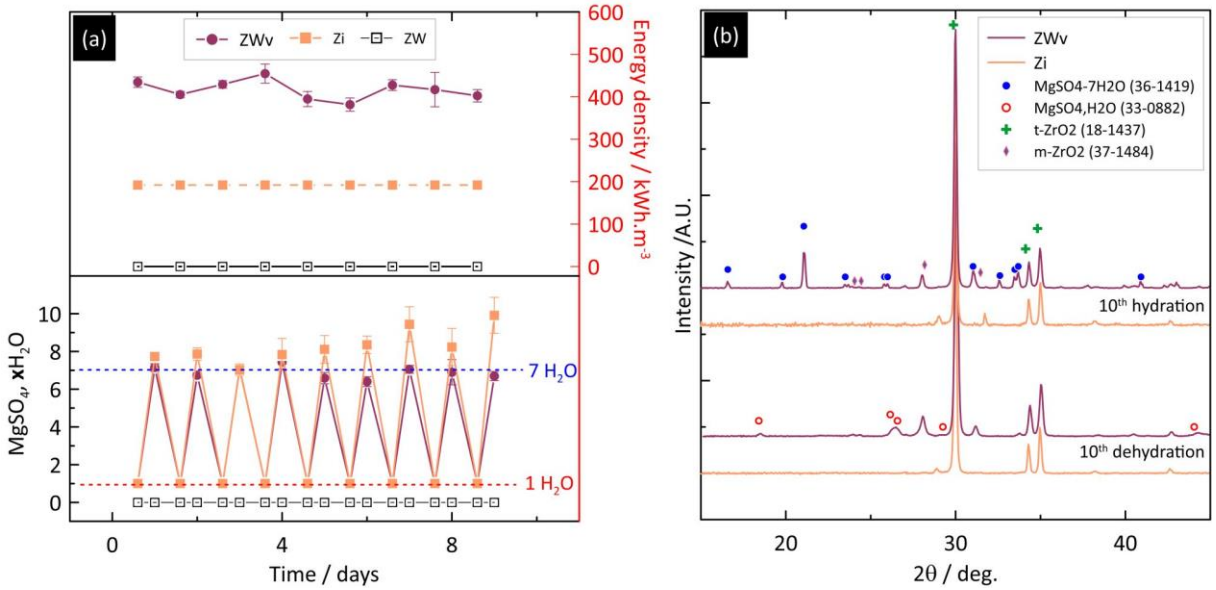

Figure 3: a. Successive hydrations of ZW, ZWv and Zi, showing a reversible behavior over time and a twice higher energy density for ZWv composite than for Zi, while ZW (without salt) does not store energy. b. Identification of the hydration state of the salt in both composites after the 10th dehydration step and after the 10th hydration step.

4. Discussion

Many different techniques already exist to create porous ceramics with hierarchical porosity [13-15]. The combination of robocasting, use of starches as pore formers and low sintering temperature is among the most powerful for at least three reasons. First, these are very simple and cost effective techniques. Second, this combination offers a large range of accessible porosities (from virtually no porosity, completely dense materials, to almost 90% porosity on different scales) using the same water-based ceramic paste (with or without starches). Third, the use of starches as pore-formers also enables taking advantage of the starch-consolidation effect: upon heating a starch-water mixture (as here during the drying phase after printing of the samples), a gelling occurs that improves the green resistance of the samples and decreases the risk of cracking during the subsequent thermal treatment steps (end of drying, debinding, sintering) [16].

Note that Pluronic® F-127 is sometimes used in the literature [17] to obtain nanometric micellar structures, and might thus have led to the formation of mesopores (according to IUPAC classification). However, here the presence of these mesopores is highly unlikely: first, the sintering step at 1250° should eliminate them completely; second, on figure 3 the ZW material shows no measureable water adsorption (that should have occurred inside mesopores).

The high hierarchical porosity obtained here in sample ZW makes it highly efficient as a host material for hygroscopic salts immobilization. Indeed, the 3-scales-porosity facilitates the infiltration step. First, the small pores drive the infiltration trough capillary forces. Second, the intermediate pores act as salt solution reservoirs thus accelerate the infiltration process. Finally, the large pores enable easy access of the salt solution to the whole surface of the filaments constituting the host material. As a result, the infiltration distance through the solid is of the order of magnitude of the half filament diameter, around 200 µm only, much smaller than the capillary rise associated to the small pores (around 1 m) thus ensuring complete infiltration of the filaments. Moreover, since a saturated salt solution is used for infiltration, drying the free water of this solution leaves enough connected porosity in the hydrated salt-infiltrated composite material to enable easy water removal during dehydration and *a fortiori* access of humid air to even the center of the filament during hydration. As a result, all the

salt deposited in the composite is reactive and the energy storage capacity of the composite (to date among the largest found in the literature [8–12]) can be reversibly exploited to its maximum. In addition, this remaining intra-filament porosity is useful to accommodate the volume changes associated to hydration or dehydration of magnesium sulfate, thus to prevent cracking of the composite. Furthermore, the mechanical resistance of the host material (0.4 MPa for the least resistant material) makes it possible to pile up chunks of the host material over a few meters height without risks of crushing it, enabling the construction of large systems without processing difficulties. A last but not least benefit of the host material is that the salt is efficiently trapped in its porosity: this prevents its global agglomeration and explains the stable dehydration / hydration cycling capacities of the present composites. Actually, agglomeration may also take place in the composites, but the agglomerate size is then limited by the pore size, contrary to what is seen in powder beds.

For the Zi composite the absence of the intermediate porosity makes the infiltration step less efficient, and most of the salt in the Zi composite is found in a layer on top of the filaments (like it could be found in powder bed design), instead of in pores inside the filaments. Less salt is thus deposited in Zi, and the salt is more prone to cracking, agglomeration and delamination from the host material (Fig 2a). Due to the thin salt layer the properties of Zi after 10 cycles do not seem to be affected, however the composite degradation is macroscopically visible on the cycled samples and the over 7 water molecules measured (Fig 3.a) indicate salt deliquescence. This confirms the interest of the hierarchical organization of the three levels of porosity, all the more that the processing technique and obtained mechanical properties enable easy upscaling of this system.

Conclusion

The 300 $kWh \cdot m^{-3}$ energy density targeted by EU for energy storage system can be reached. We show here that using a host material with high, optimized, hierarchical porosity to trap magnesium sulfate can lead to energy density as high as 420 $kWh \cdot m^{-3}$, with complete stability over time, demonstrated by 10 cycles of dehydration and hydration (or 10 years in terms of inter-seasonal energy storage). These structures are obtained by a combination of ceramic 3D-printing (robocasting), starch as pore-former materials and partial sintering. Their high thermal efficiency is related in particular to their hierarchical porosity that allows easy salt infiltration and efficient salt trapping without global agglomeration while the still incomplete infiltration enables the whole volume of salt to be active in the hydration / dehydration process, thus maximizes the energy storage capacity, while preventing cracking upon hydration / dehydration cycles.

Acknowledgments

This work is part of DECARTH project and is financially supported by the French national research agency (ANR) (grant number ANR-16-CE22-0006).

Data availability

The raw/processed data required to reproduce these findings cannot be shared at this time as the data also forms part of an ongoing study.

References

[1] ADEME, Actualisation Du Scénario Énergie-Climat ADEME 2035-2050, 2017. ISBN 9791029709210

[2] Directive (EU) 2018/2001 of the European Parliament and of the Council of 11 December 2018 on the Promotion of the Use of Energy from Renewable Sources, Official Journal Of The European Union, 2018.

[3] J. C. Hadorn, Thermal Energy Storage for Solar and Low Energy Building: State of the Art by the IEA solar heating and cooling task 32, 2005.

[4] A. Abedin, M. Rosen, A Critical Review of Thermochemical Energy Storage Systems. *Open Renew. Energy J.* 4 (2011), 42-46. https://doi.org/10.2174/1876387101004010042

[5] L. Scapino, H. A. Zondag, J. Van Bael, J. Diriken, C. C. M. Rindt, Sorption heat storage for long-term low-temperature applications: A review on the advancements at material and prototype scale. *Appl. Energy* 190 (2017), 920-948. https://doi.org/10.1016/j.apenergy.2016.12.148

[6] European Technology Platform on Renewable Heating: Strategic Research Priorities for Solar Thermal Technology, 2012.

[7] K. E. N'Tsoukpoe, H. Liu, N. Le Pierrès, L. Luo, A review on long-term sorption solar energy storage, *Renew. Sustain. Energy Rev.* 13 (2009), 2385-2396. https://doi.org/10.1016/j.rser.2009.05.008

[8] S. Mauran, H. Lahmidi, V. Goetz, Solar heating and cooling by a thermochemical process. First experiments of a prototype storing 60 kW h by a solid/gas reaction, *Sol. Energy* 82 (2008), 623-636. https://doi.org/10.1016/j.solener.2008.01.002

[9] N. Le Pierrès, N. Mazet, D. Stitou, Experimental results of a solar powered cooling system at low temperature. *Int. J. Refrig.* 30 (2007), 1050-1058. https://doi.org/10.1016/j.ijrefrig.2007.01.002

[10] B. Michel, Procédé Thermochimique Pour Le Stockage Intersaisonnier de l'énergie Solaire : Modélisation Multi-Échelles et Expérimentation d'un Prototype Sous Air Humide, PhD thesis, Perpignan, France, 2012.

[11] S. Hongois, F. Kuznik, P. Stevens, J. J. Roux, Development and characterisation of a new MgSO4-zeolite composite for long-term thermal energy storage. *Sol. Energy Mater. Sol. Cells* 95 (2011), 1831-37. https://doi/org/10.1016/j.solmat.2011.01.050

[12] L. Okhrimenko, Stockage d'énergie Thermique Par Un Composite Zéolite/MgSO4 : Étude Thermocinétique Du Système MgSO4 – H2O et Étude Expérimentale Des Composites, PhD thesis, Ecole des Mines de Saint Etienne, France, 2018.

[13] T. Ohji, M. Fukushima, Macro-porous ceramics: Processing and properties. *Int. Mater. Rev.* 57 (2012), 115-131.https://doi.org/10.1179/1743280411Y.0000000006

[14] E. C. Hammel, O. L. R. Ighodaro, O. I. Okoli, Processing and properties of advanced porous ceramics: An application based review. *Ceram. Int.* 40 (2014), 15341-15370. https://doi.org/10.1016/j.ceramint.2014.06.095

[15] D. Jang, L. R. Meza, F. Greer, J. R. Greer, Fabrication and deformation of three-dimensional hollow ceramic nanostructures. *Nat. Mater.* 12 (2013), 893-898. https://doi/org/10.1038/nmat3738

[16] O. Lyckfeldt, J. M. F. Ferreira, Processing of porous ceramics by 'starch consolidation', *J. Eur. Ceram. Soc.* 18 (2002), 131-140. https://doi.org/10.1016/s0955-2219(97)00101-5

[17] Z. Song, H. Duan, D. Zhu , Y. Lv , W. Xiong , T. Cao, L. Li , M. Liu, L. Gan, Ternary-doped carbon electrodes for advanced aqueous solid-state supercapacitors based on a "water-in-salt" gel electrolyte, *J. Mater. Chem. A* 7 (2019), 15801-15811. https://doi-org /10.1039/C9TA02690H